A&A 370, 881–899 (2001)
DOI: 10.1051/0004-6361:20010288

Astronomy & Astrophysics

Near-infrared observations of galaxies in Pisces-Perseus

IV. Color maps of 41 cluster spirals⋆

G. Moriondo[1], C. Baffa[1], S. Casertano[2], G. Chincarini[3], G. Gavazzi[4], C. Giovanardi[1], L. K. Hunt[5], D. Pierini[6], M. Sperandio[3], and G. Trinchieri[7]

[1] Osservatorio Astrofisico di Arcetri, Largo E. Fermi 5, 50125 Firenze, Italy
[2] Space Telescope Science Inst., 3700 San Martin Drive, Baltimore, MD 21218, USA
[3] Osservatorio Astronomico di Brera, Via E. Bianchi 46, 22055 Merate (CO), Italy
[4] Dipartimento di Fisica, Sez. Astrofisica, Università di Milano, Via Celoria 16, 20133 Milano, Italy
[5] C.A.I.S.M.I-C.N.R., Largo E. Fermi 5, 50125 Firenze, Italy
[6] Department of Physics and Astronomy, University of Toledo, 2801 W. Bancroft, Toledo, OH 43606, USA
[7] Osservatorio Astronomico di Brera, Via Brera 28, 20121 Milano, Italy

Received 25 October 2000 / Accepted 16 February 2001

Abstract. We present near-infrared (NIR) color maps of a sample of 41 disk galaxies in the Pisces-Perseus supercluster. The sample objects, mainly members of the Pisces cluster, are a subset of larger sample imaged in the H band. For most objects we present $J-H$ and $J-K$ images and elliptically-averaged radial color profiles; for some objects this is done only for the $H-K$ color. We compute global colors, hybrid NIR-optical colors, and estimate the colors of the structural components. The $J-K$ (global) color correlates weakly with absolute luminosity and morphological type. We observe no trend with the presence of bars and AGNs, nor with position within the cluster. The NIR disk colors are slightly bluer than the global ones, with the possible exception of those in the earliest spiral types. Finally, NIR color gradients in the images and in the radial color profiles are examined. NIR disk color gradients are small and prevalently negative; the few positive values are perhaps associated with the reddest disks.

Key words. galaxies: fundamental parameters – galaxies: spiral – infrared: galaxies

1. Introduction

This paper is part of a series concerning near-infrared (NIR) observations of disk galaxies in the Pisces-Perseus supercluster. In Paper I (Moriondo et al. 1999a) we presented the H-band (1.64 μm) images of 174 spirals. These data were used in Paper II (Moriondo et al. 1998b) to investigate internal extinction effects, and in Paper III (Moriondo et al. 1999b) in the framework of distance indicators.

In the course of the observations described in Paper I, a number of these galaxies have been imaged in passbands other than H. Namely, we have J, H, and K images for 34 of them plus H and K only for 7 more galaxies. This paper presents the color images obtained and the results of their analysis.

2. Sample and observations

The basic data of the sample objects, as listed in NED[1], are summarized in Table 1; their positions are depicted in Fig. 1, and their morphological distribution is illustrated in Fig. 2. The entries in Table 1 are as follows. *Column 1*: UGC[2] number or, if missing, CGCG[3] number. *Column 2*: Other common names. *Columns 3 and 4*: J2000 equatorial coordinates. *Column 5*: Revised Hubble morphological type. *Column 6*: Blue total magnitude in the

Send offprint requests to: C. Giovanardi,
e-mail: giova@arcetri.astro.it

⋆ Based on observations at the TIRGO, NOT, and VATT telescopes. TIRGO (Gornergrat, CH) is operated by CAISMI-CNR, Arcetri, Firenze. NOT (La Palma, Canary Islands) is operated by NOTSA, the Nordic Observatory Scientific Association. VATT (Mt. Graham, Az) is operated by VORG, the Vatican Observatory Research Group.

[1] This research has made use of the NASA/IPAC Extragalactic Database (NED) which is operated by the Jet Propulsion Laboratory, California Institute of Technology, under contract with the National Aeronautics and Space Administration.

[2] Uppsala General Catalogue of Galaxies (Nilson 1973).

[3] Catalogue of Galaxies and Clusters of Galaxies (Zwicky et al. 1961–68).

Table 1. General data of the sample galaxies

Names		R.A. (J2000)	Dec.	RH Type	m_B	Size	V_H	Notes
		[h m s]	[° ' "]		[mag]	[arcmin]	[km s^{-1}]	
(1)	(2)	(3)	(4)	(5)	(6)	(7)	(8)	(9)
UGC 12914	(VV 254)	00 01 38.2	23 29 04	(R)S(r)cd:	13.1	2.3x1.3	4371	
UGC 12915	(VV 254)	00 01 42.1	23 29 42	S?	13.9	1.5x0.5	4336	
UGC 00365	NGC 0169	00 36 52.0	23 59 30	SA(s)ab:	13.3	2.6x0.7	4627	sp
UGC 00646		01 03 26.5	32 14 15	SB?	14.8	1.2x0.5	5319	
UGC 00673		01 06 09.7	31 24 24	SAc?	15.7	1.3x0.5	6254	pure disk
CGCG 501-091		01 07 57.5	33 18 12	S?	15.2	0.9x0.7	4209	
UGC 00697		01 08 04.8	33 27 10	SB?	14.7	0.9x0.5	4647	
UGC 00710		01 08 44.6	33 27 53	Sbc	15.3	1.4x0.5	12471	
UGC 00714		01 09 14.0	32 09 04	SAc	14.3	1.1x0.9	4634	
UGC 00732		01 10 44.4	33 33 28	SA(r)d	14.6	1.0x0.6	5436	
UGC 00738		01 11 04.9	33 50 05	Sdm	15.0	1.2x1.1	4558	
UGC 00745		01 11 30.1	36 40 39	Scd:	16.5	0.9x0.4	9629	pure disk
UGC 00776	NGC 0431	01 14 04.6	33 42 13	SB0	13.9	1.4x0.9	5786	
UGC 00798	IC 1654	01 15 11.9	30 11 41	(R)SB(r)a	14.1	1.3x1.2	4897	
UGC 00800		01 15 19.2	28 29 24	Scd:	14.9	0.9x0.8	4812	pure disk
UGC 00820	NGC 0452	01 16 14.8	31 02 01	SBab	13.6	2.5x0.8	4962	
CGCG 502-021		01 16 33.1	28 58 31	S?	15.4	0.7x0.5	8170	
UGC 00831		01 18 10.0	38 26 38	S?	14.8	1.1x0.7	7286	
UGC 00835		01 18 40.1	31 02 11	Scd:	14.6	1.0x0.8	6834	
CGCG 502-032	IC 1669	01 20 06.4	33 11 07	Sa	15.6	1.0x0.3	5717	
UGC 00909		01 22 01.4	37 24 02	Sd	14.1	1.6x1.1	5084	
UGC 00911		01 22 09.9	32 12 56	SBb	14.9	0.8x0.7	10552	
UGC 00919	NGC 0494	01 22 55.4	33 10 26	Sab	13.8	2.0x0.8	5462	
UGC 00927	NGC 0496	01 23 11.5	33 31 46	Sbc	14.1	1.6x0.9	6006	
UGC 00937		01 23 37.5	32 37 48	S?	15.0	0.7x0.5	4748	pure disk
UGC 00940		01 23 37.9	34 34 11	SA(s)c	15.1	1.0x0.7	6996	
UGC 00975		01 25 15.6	34 21 34	S	15.0	1.2x0.8	4897	
UGC 01013	NGC 0536	01 26 21.6	34 42 14	SB(r)b	13.2	3.0x1.1	5189	
CGCG 502-085	MRK0358	01 26 33.6	31 36 59	SAB(rs)bc:	14.8	0.9x0.7	13550	Sy1
UGC 01034	NGC 0551	01 27 40.6	37 10 58	SBbc	13.5	1.8x0.8	5189	
CGCG 521-038	VV597	01 29 40.4	33 49 52	S	15.3	0.8x0.8	6575	pure disk
CGCG 502-097		01 29 46.1	32 01 12	S	15.6	0.8x0.3	6341	pure disk
UGC 01100	NGC 0587	01 32 33.3	35 21 31	SAB(s)b	13.6	2.2x0.8	4530	
UGC 01111	NGC 0591	01 33 31.2	35 40 06	(R')SB0/a	13.9	1.3x1.0	4547	Sy2
UGC 01131		01 35 16.4	34 28 21	SABdm:	15.0	1.1x1.0	5086	
CGCG 521-068		01 41 15.3	34 48 43	SB?	14.8	0.5x0.5	5092	
CGCG 503-007		01 42 51.2	31 29 06	S?	15.5	0.5x0.5	10432	pure disk
UGC 01437	NGC 0753	01 57 42.4	35 54 57	SAB(rs)bc	13.0	2.5x1.9	4903	
UGC 01633	NGC 0818	02 08 44.4	38 46 36	SABc:	13.2	3.0x1.3	4246	
UGC 01935	NGC 0931	02 28 14.5	31 18 42	Sbc	14.5	3.9x0.8	5004	Sy1.5
UGC 02548	NGC 1207	03 08 15.3	38 22 57	SA(rs)b	13.4	2.3x1.7	4800	

B_T system. *Column 7*: Optical major and minor axes in arcmin. *Column 8*: Systemic heliocentric velocity. *Column 9*: Peculiarities or comments; the meaning of the label "pure disk" is explained in Sect. 3.2. As shown in Fig. 1, the present sample does not cover the entire supercluster area, as was the case for the whole sample of Paper I, since it was devised to study in more detail the members of the Pisces cluster and its immediate neighborhood. The morphological distribution, shown in the lower panel of Fig. 2, is also different: first, it is more uniform and not as strongly peaked between $T = 3$ and 6 as for the sample in Paper I; second, it contains a larger number of uncertain spiral types. The present sample is in fact fainter, $\langle m_B \rangle = 14.50$ against 13.92 of the whole set, a consequence of the choice of retaining the bulk of the background objects; of the 41 galaxies in the present sample, 10 have velocities in excess of 6500 km s^{-1}. The upper panel of the same figure illustrates the distribution of absolute B magnitudes among the various types, with the customary decline in

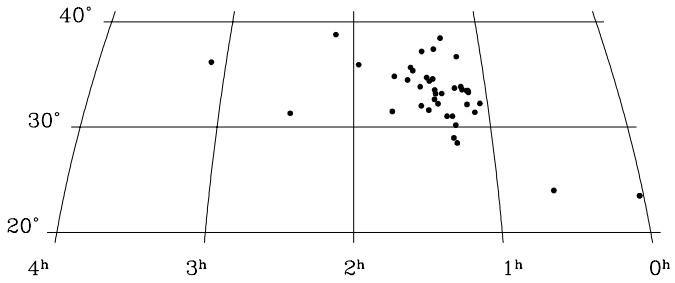

Fig. 1. Position of the sample objects in equatorial coordinates (equal-area projection)

luminosity towards later types[4]. Here the absolute magnitudes are computed from the $m_{\rm B}$ value listed in Table 1 and a plain redshift distance with $H_0 = 75\,{\rm km\,s^{-1}\,Mpc^{-1}}$.

The observations and data reduction are described in detail in Paper I, where the interested reader can also find a discussion of their accuracy and comparisons with previous photometric studies. The information given there refers to the H-band data; however, in terms of Zero-Point stability and seeing characteristics, no systematic differences were discernible among the three passbands. All image reduction was performed with IRAF and the STSDAS packages[5]. As in Paper I, all the data presented here take into account only correction for atmospheric extinction; no correction has been applied for Galactic or internal extinction nor for the effects of redshift (K correction, and angular-size $-$ z relation). An estimate of the magnitude of these corrections is given in Sect. 3.1.

3. Results

The color images are shown in Fig. 3 together with the elliptically averaged radial color profiles. We report results for $J-H$ and $J-K$ except for the cases where we have data for $H-K$ only. The color images are obtained by subtracting surface magnitude images in the various bandpasses after degradation of the image with better seeing to the seeing value of the worse image.

In order to improve the appearance of the color images, they have also been smoothed in the outer regions; namely, no smoothing is applied to the regions where the H-band surface magnitude μ_H is brighter than 17.5 mag arcsec^{-2}; a Gaussian smoothing with $\sigma = 0.75$ arcsec is applied for $17.5 < \mu_H < 18.5$; and a Gaussian smoothing with $\sigma = 1.5$ arcsec is applied for $\mu_H > 18.5$. To derive the radial profiles, elliptical isophotes with fixed center, but variable ellipticity and position angle, were first fitted to the H-band image; this was performed in linear steps of 1 pixel for semimajor axes from 1 to 10 pixels, and then outward in geometric progression with 15% increase between steps. This same set of elliptical apertures was then applied to the J- and K-band image to derive the corresponding color profiles. The choice of letting the ellipticity and position angle vary with galactocentric distance yields color profiles which better represent the true local colors and those of the structural components.

[4] Inspection of the POSS II suggests that the low-luminosity Sa (CGCG 502-302, $M_B = -18.8$) is most probably missclassified.

[5] IRAF is the Image Analysis and Reduction Facility made available to the astronomical community by the National Optical Astronomy Observatories, which are operated by AURA, Inc., under contract with the U.S. National Science Foundation. STSDAS is distributed by the Space Telescope Science Institute, which is operated by the Association of Universities for Research in Astronomy (AURA), Inc., under NASA contract NAS 5–26555.

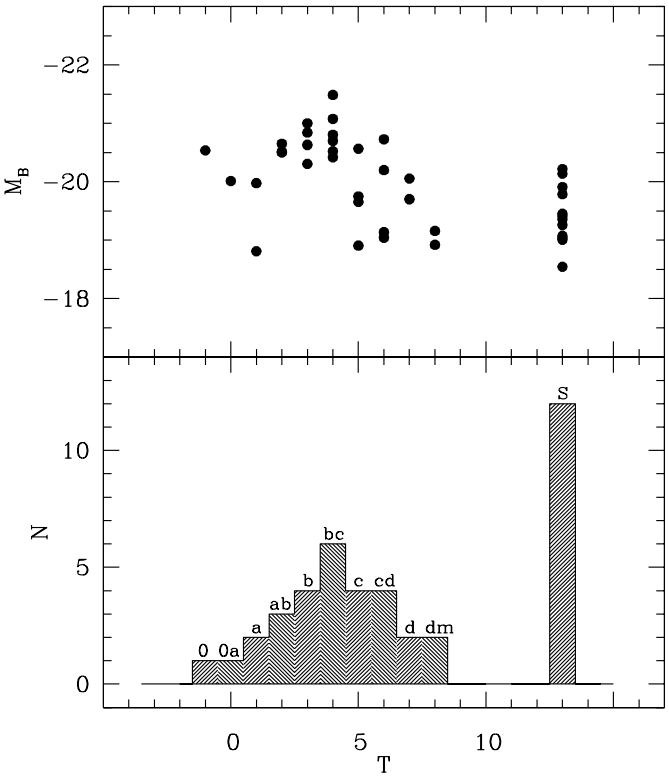

Fig. 2. In the lower panel: morphological distribution of the sample galaxies. N is the number of objects per RH classification bin, T is the index of stage along the Hubble sequence from the RC3. Spiral types are also reported on top of each bin. The rightmost bin, coded S, refers to objects classified S or SB without further specification. In the upper panel: absolute B magnitudes vs. T

3.1. Global colors

For each galaxy we have computed global colors. These are defined as the differences between the magnitudes in the various passbands measured within the elliptical isophote at 21.5 H-mag arcsec^{-2}; we indicate them as $(J-H)_{21.5}$, $(J-K)_{21.5}$, and $(H-K)_{21.5}$. As noted in Paper I, this procedure provides more stable and reliable measurements than using total, extrapolated magnitudes. The uncertainties are largely dominated by those in the photometric calibration and, therefore, the reported errors on the colors take into account the scatter of the Zero Points in the various bands. Table 2 reports these isophotal colors and their 1σ uncertainty: *Columns* 2 and 3 give, respectively, the isophotal magnitude and the major axis in arcmin for the elliptical isophote at 21.5 H-mag arcsec^{-2} (from Paper I); *Column* 4 $r_{\rm BD}$, the transition radius in arcmin between bulge and disk (see Sect. 3.2); *Columns* 5 and 6 give the two global colors $(J-H)_{21.5}$ and $(H-K)_{21.5}$; $\sigma(J-K)_{21.5}$ in *Column* 7 is the uncertainty to be assigned to the $(J-K)_{21.5}$.

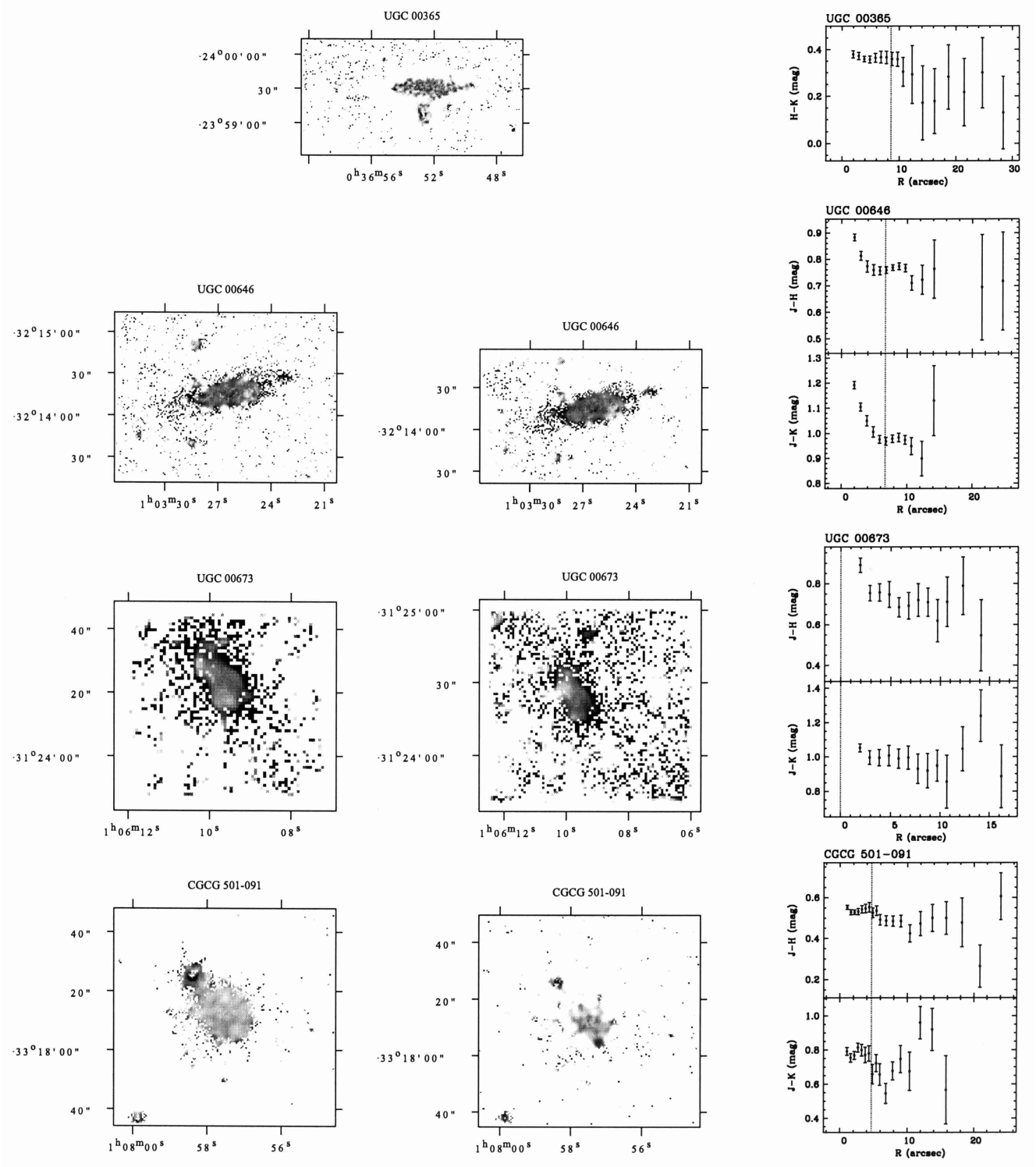

Fig. 3. Color maps and radial color profiles. If two maps are present, the left one is $J-H$ and the right one $J-K$; if one map is present it is $H-K$. The elliptically averaged radial color profiles, with 1σ errorbars, extend to the point where the error is 0.2 mag. The vertical dotted line marks the radius where the disk becomes dominant, as defined in the text

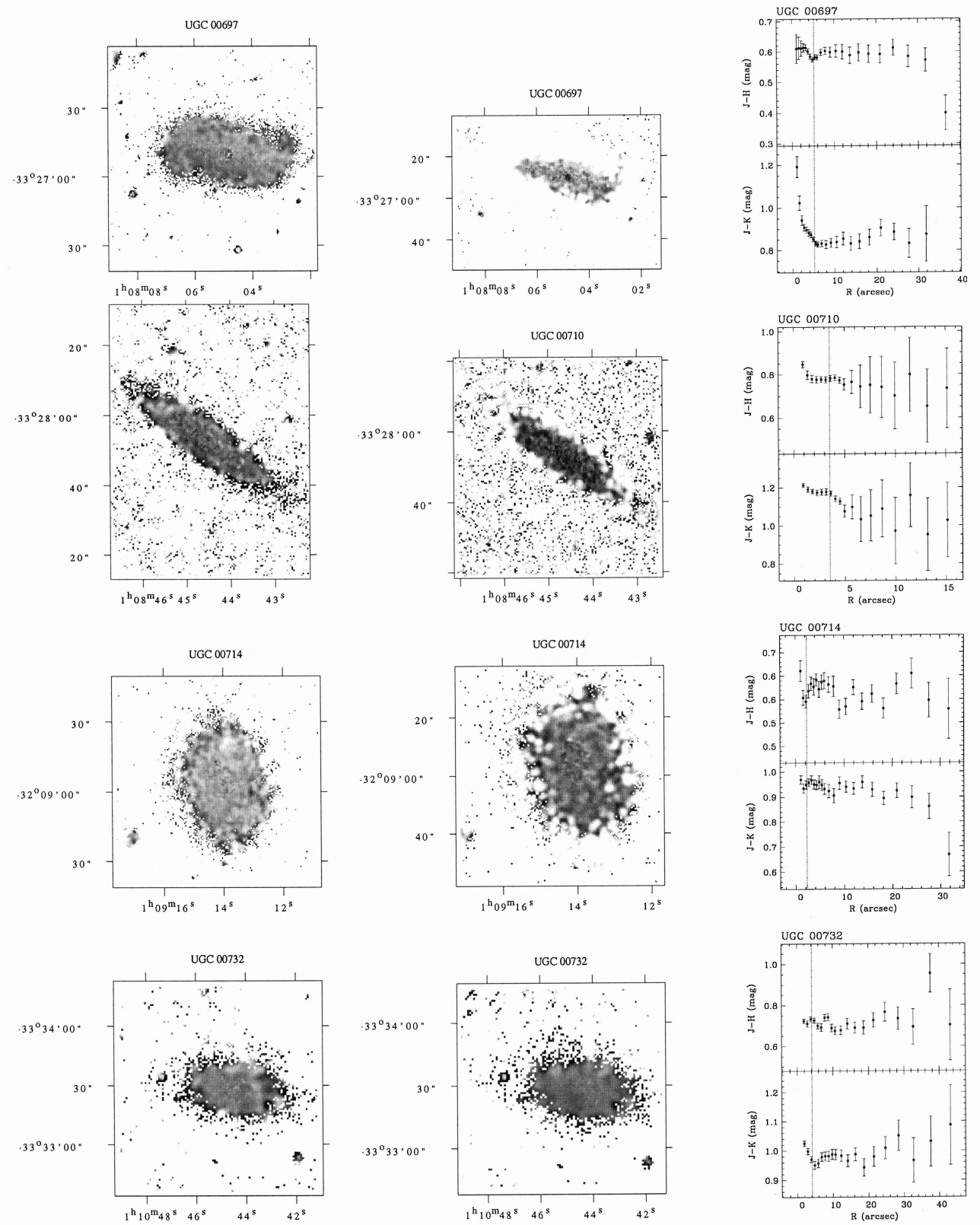

Fig. 3. continued

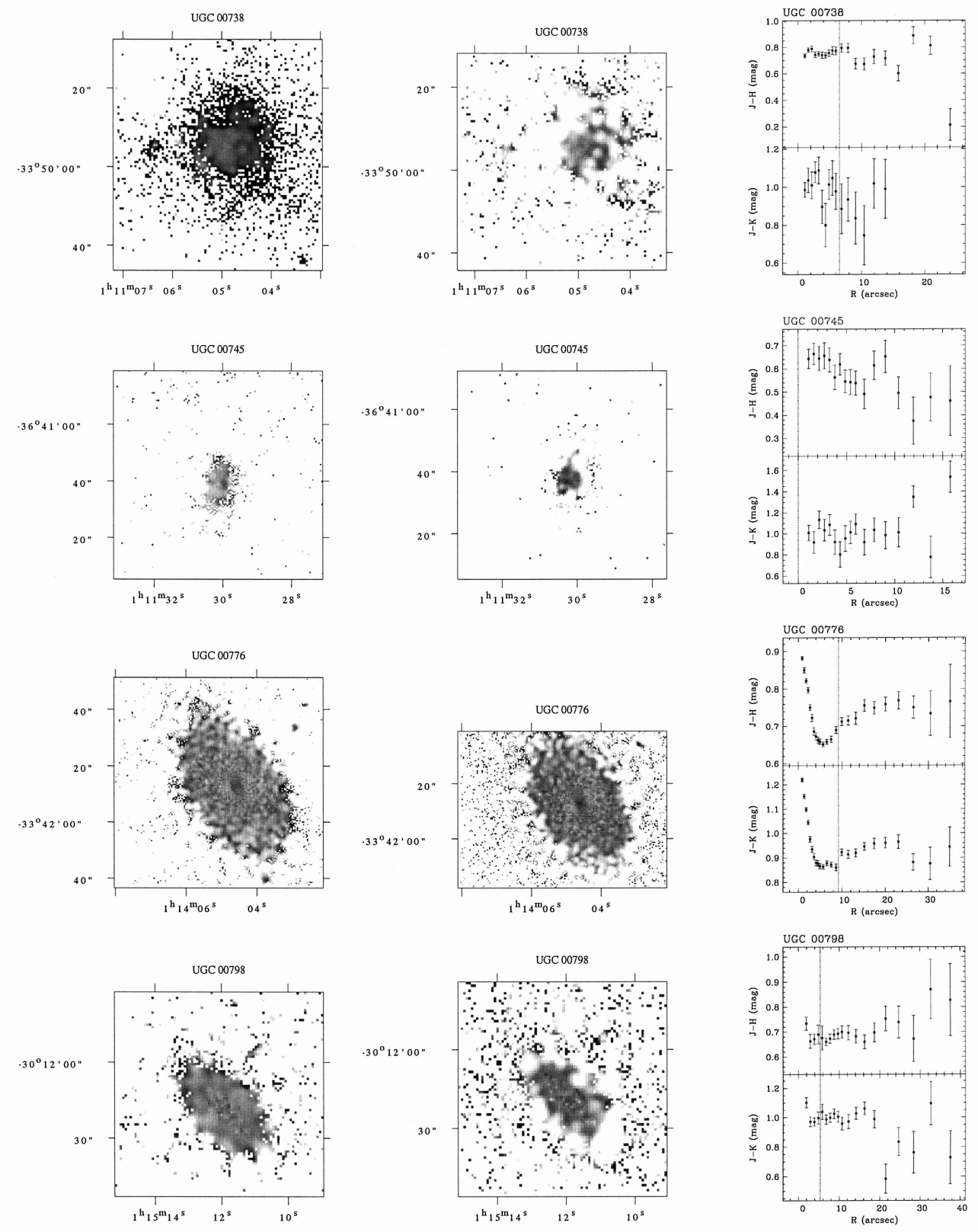

Fig. 3. continued

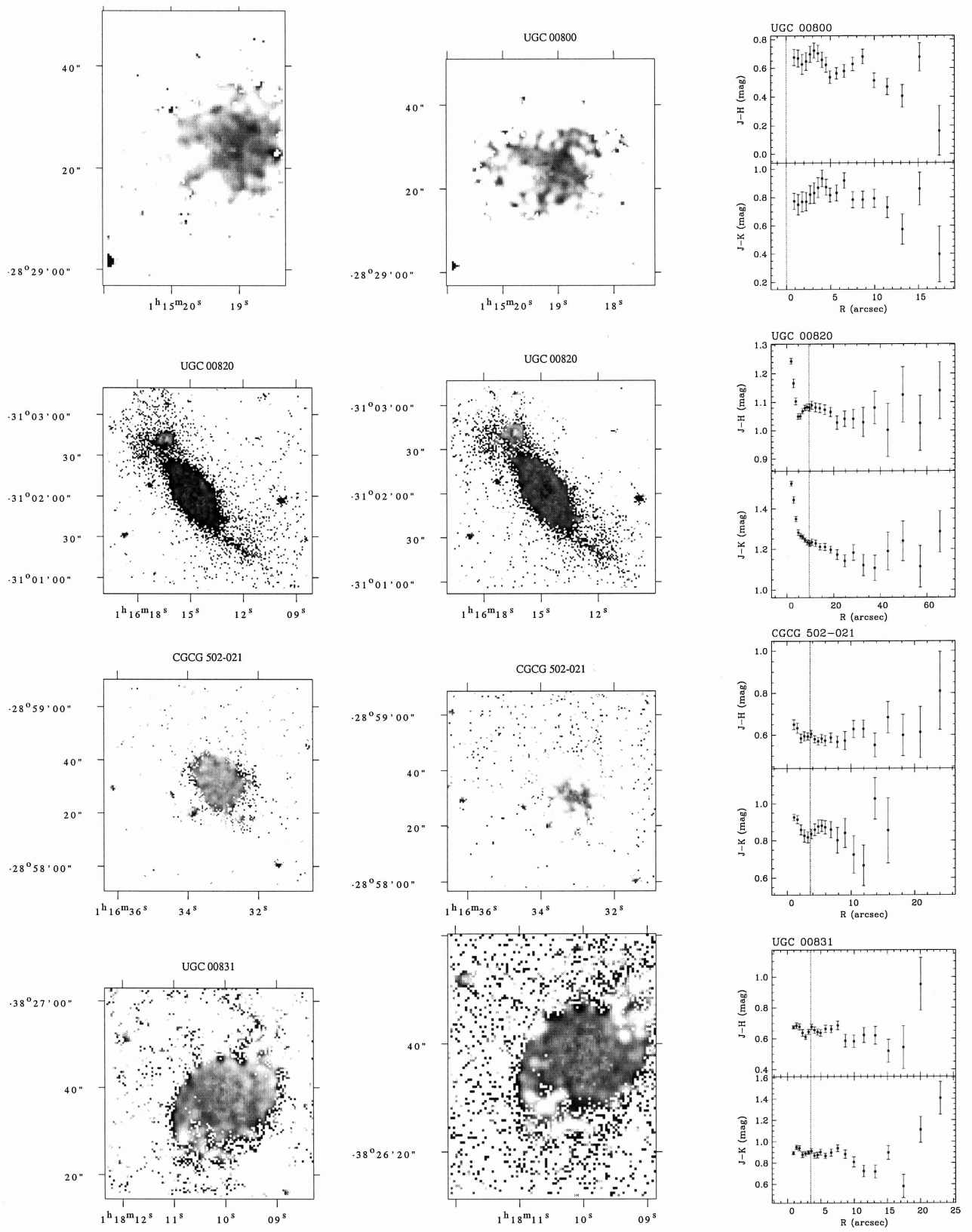

Fig. 3. continued

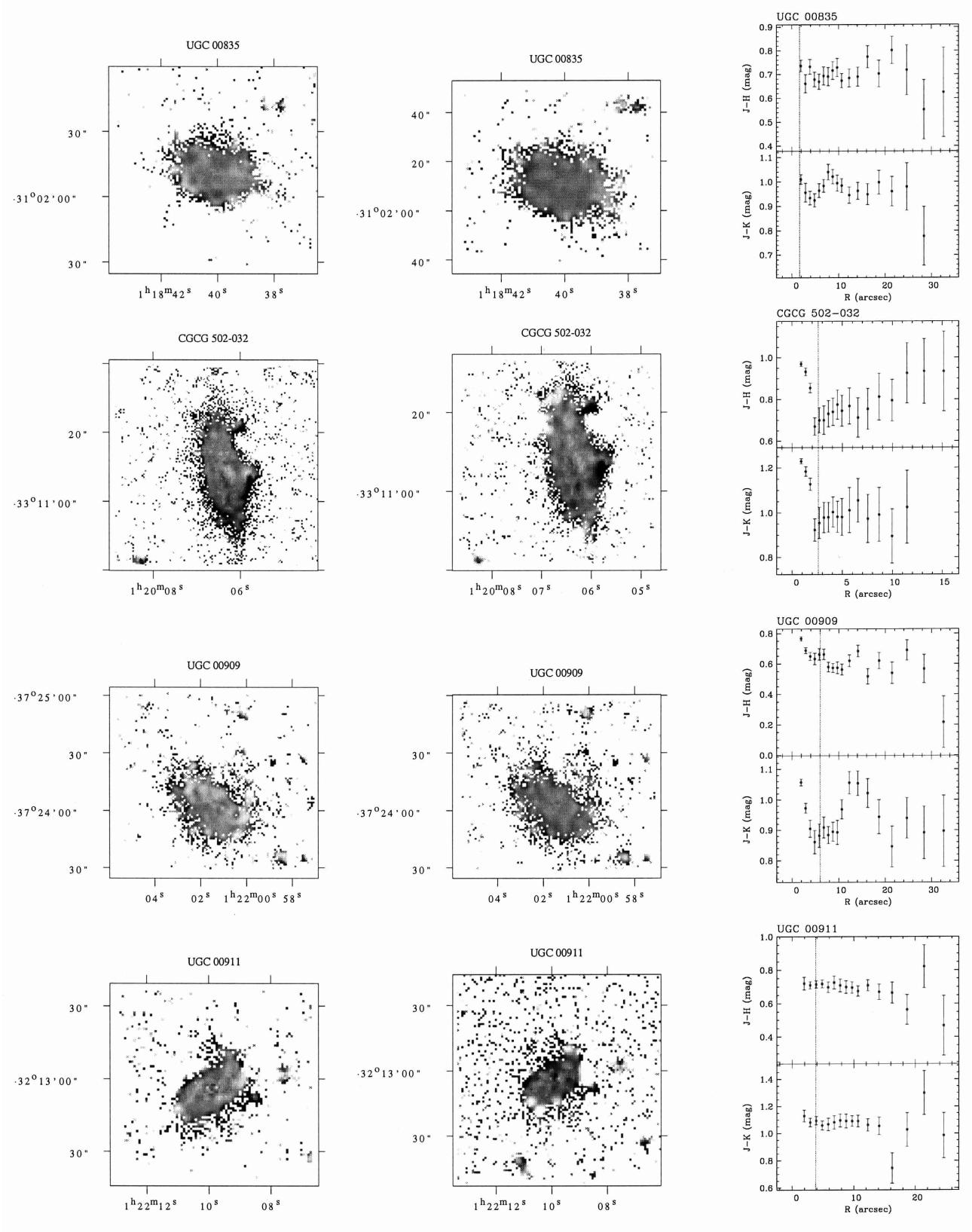

Fig. 3. continued

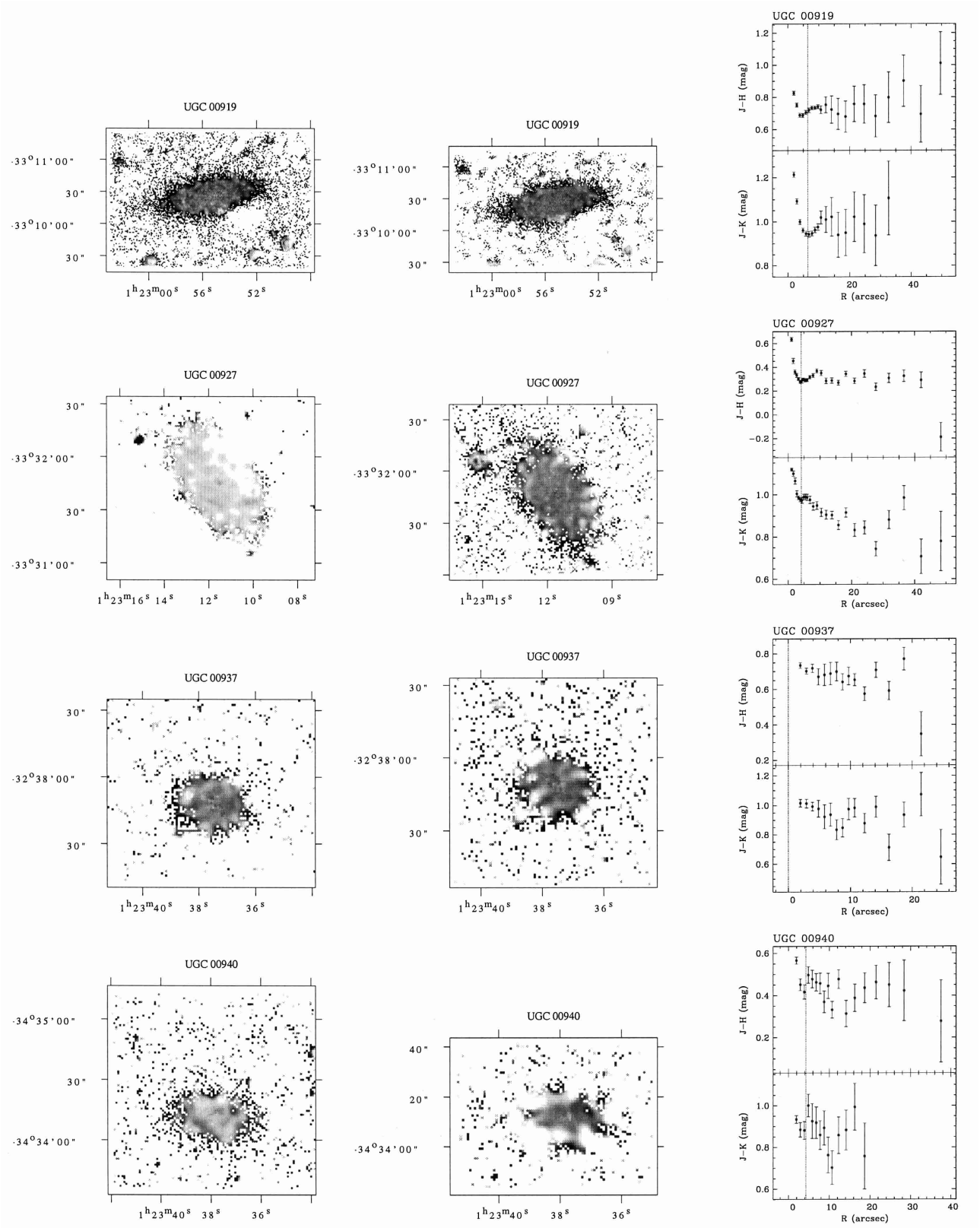

Fig. 3. continued

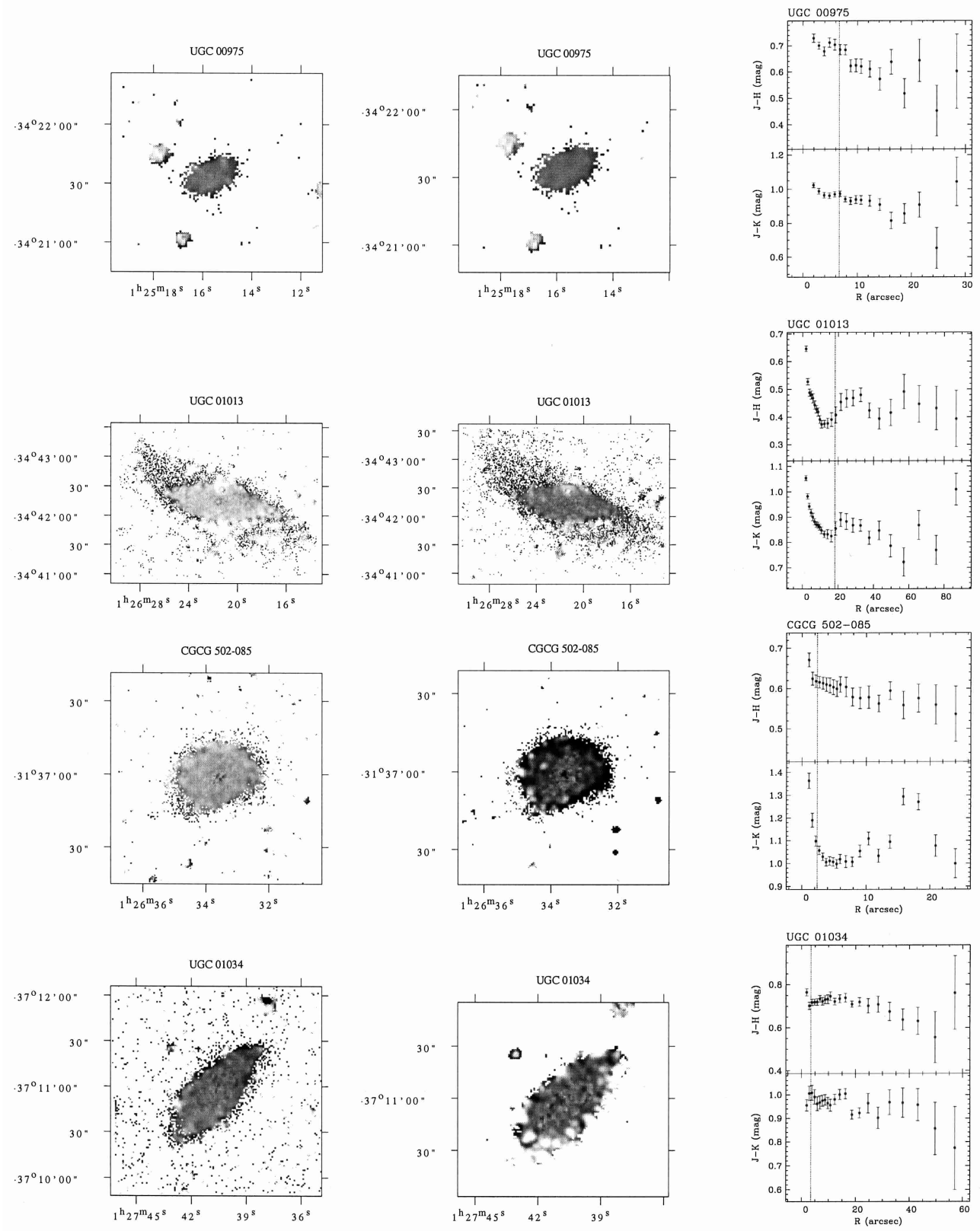

Fig. 3. continued

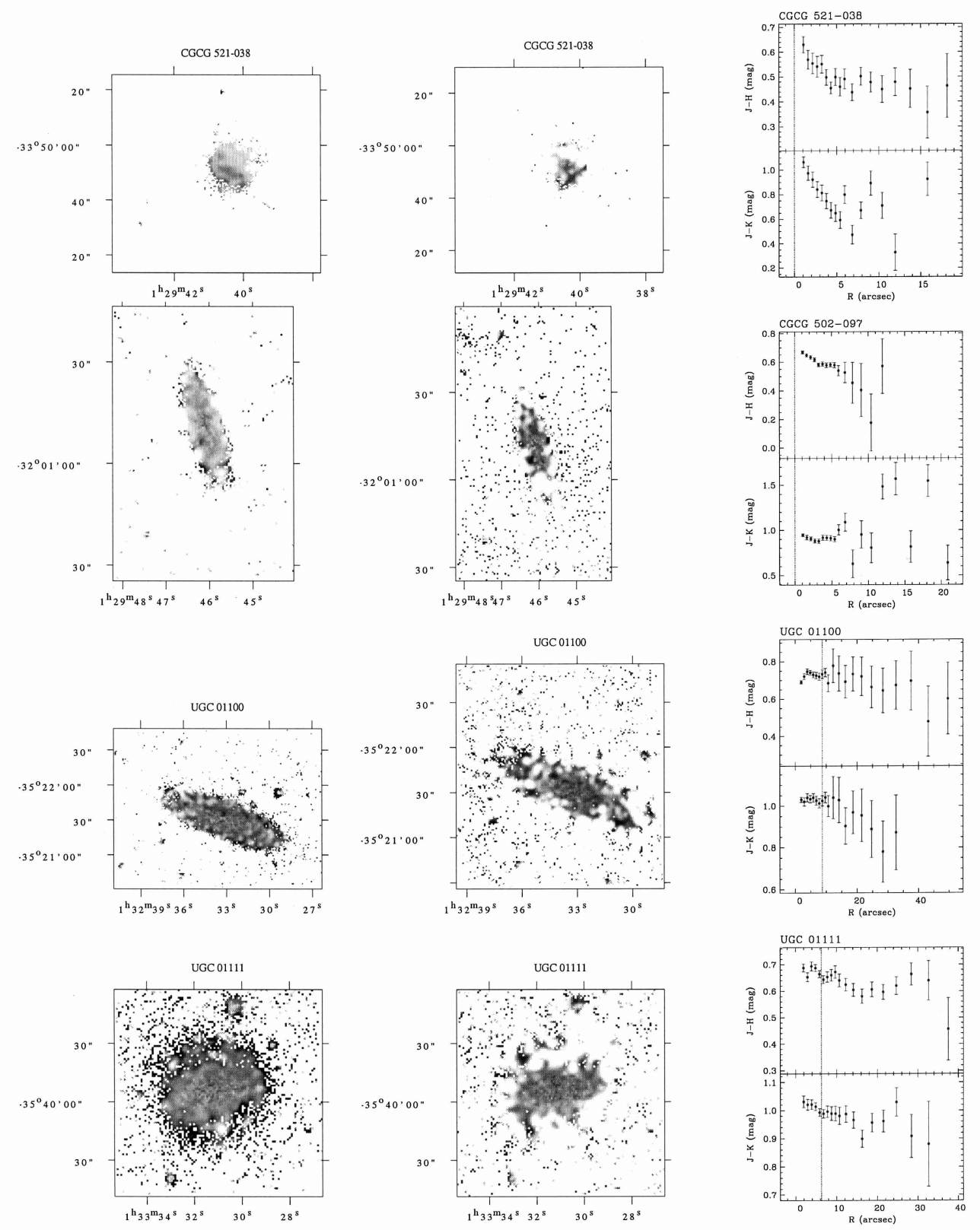

Fig. 3. continued

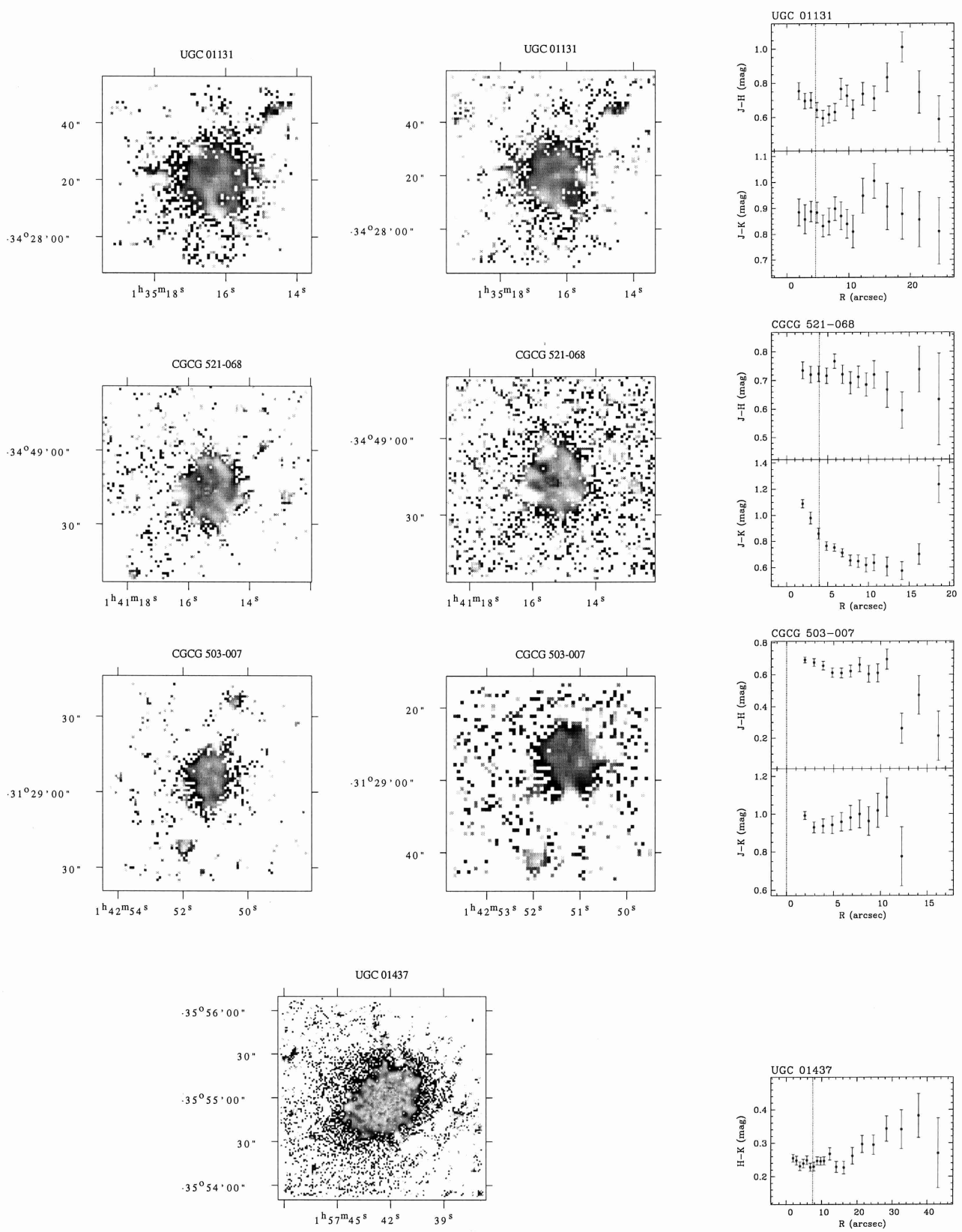

Fig. 3. continued

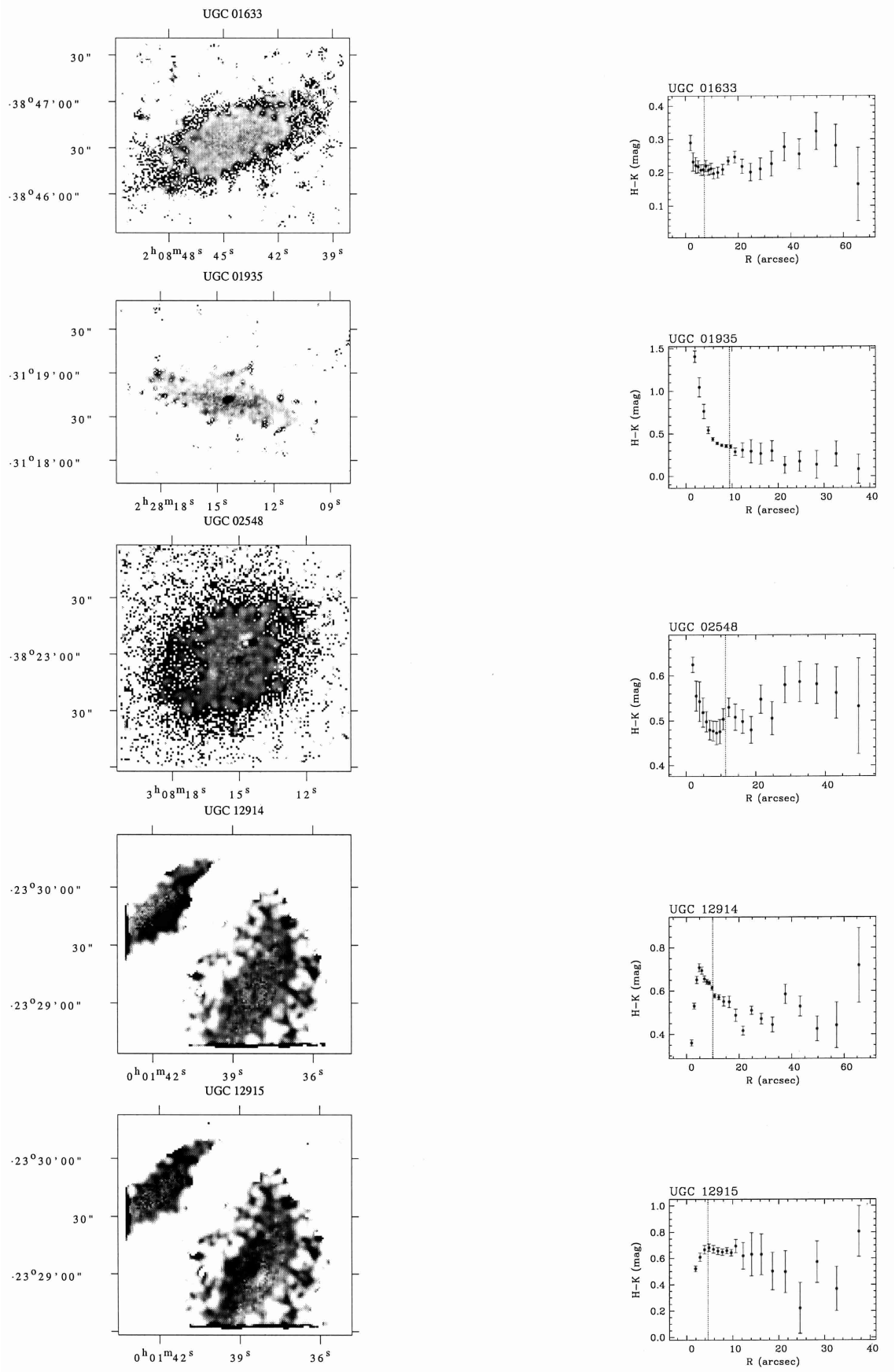

Fig. 3. continued

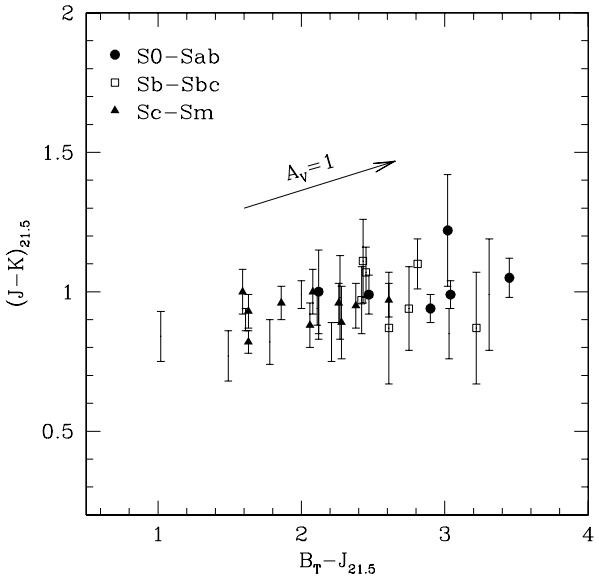

Fig. 4. NIR global color $(J-K)_{21.5}$ vs. the optical-NIR color $B_{\rm T}-J_{21.5}$ for the sample objects. Different symbols refer, as indicated, to different morphologies; no symbol is used in case of classification as S or SB without further specification. The arrow shows the reddening line according to Cardelli et al. (1989)

In addition to the NIR colors we can produce a rough estimate of the optical-NIR color by using the $m_{\rm B}$ magnitude available from catalogues (NED) and listed in Table 1. Figure 4 shows the color-color diagram using the NIR $(J-K)_{21.5}$ vs. the hybrid $B_{\rm T}-J_{21.5}$[6]. It can be seen that, while later morphologies tend to bluer $B_{\rm T}-J_{21.5}$ indices, no such effect is evident in $(J-K)_{21.5}$; this confirms the only weak dependence, in normal spirals, of the NIR emission on recent star formation episodes and its link to the red giant population (Frogel 1985). As seen in Fig. 4, the distribution in the color-color plot is elongated along the direction of a typical reddening line, in this case the one of Cardelli et al. (1989). This suggests that, at least within the same morphological type, the photometric properties are strongly bound to the internal extinction, detectable still at NIR wavelengths; this issue has been investigated in the second paper of this series (Moriondo et al. 1998b).

The average global colors for the whole sample are $\langle\ J-H\ \rangle_{21.5} = 0.67 \pm 0.12$ and $\langle\ H-K\ \rangle_{21.5} = 0.31 \pm 0.11$, in agreement with previous studies (e.g. Griersmith et al. 1982). Not applying a K-correction results in colors which are redder than their intrinsic (rest frame) value; at the average systemic velocity of our sample (6050 km s^{-1}), the correction amounts to -0.01 and -0.07 for $J-H$ and $H-K$ respectively (Frogel et al. 1978). As for the reddening within our Galaxy, for an average $A_{\rm V}=0.12$ mag in this area, the corrections are about -0.01 in both colors. The observed global colors are only slightly bluer than the colors observed within small (5–10 arcsec) apertures. For example, Willner et al. (1984) quote 0.77 ± 0.02 and 0.26 ± 0.05, for $J-H$ and $H-K$ respectively, within an aperture ($8''$) corresponding to linear sizes of 0.5–1.0 kpc.

The left panel of Fig. 5 shows a plot of the $(J-K)_{21.5}$ vs. the absolute H magnitude, obtained using $H_{21.5}$ (from Paper I) and redshift distances for an $H_0=75$ km s^{-1} Mpc^{-1}. This plot may be compared with the one in the lower panel of Fig. 7 in Paper I showing the color-luminosity relation using the hybrid $m_{\rm B}-H_{\rm T}$: despite the short wavelength leverage, the correlation for $(J-K)_{21.5}$ is not worse than the hybrid one. This is partly due to the lower errors in $(J-K)_{21.5}$, but mainly to the tight spread at a given luminosity of the NIR colors.

The NIR color-color diagram is shown in Fig. 6 for the global colors in the right panel, and for the disks, as explained in Sect. 3.2, in the left one. For a better comparison with stellar colors, the values plotted in Fig. 6 have been corrected for K-dimming and Galactic extinction[7]. The apparent anticorrelation between $J-H$ and $H-K$, in both the global and the disk plot, is due to points with quite large photometric errors. Taking into account the uncertainties of the single data points, a linear correlation analysis yields a slope of -0.75 ± 0.35 and a correlation coefficient of -0.46. By excluding the three points with the largest errors, the slope becomes -0.96 ± 0.56 and the coefficient -0.30. The correlation should then be regarded as dubious. The objects with the most extreme and uncertain colors ($0.5 > (J-H)_{21.5} > 0.9$) are normal spirals of different types (UGC 820, 927, 940, and 1013). As reported in the right panel, and apart from the most deviant cases, the NIR colors are characteristic of late-type stars of spectral type K0 to M5, and of any luminosity class from I to V. Again taking into account the errors assigned to the single points, only UGC 927 with (corrected) $(H-K)_{\rm D}=0.44$ $(J-H)_{\rm D}=0.29$ stands at more than 1.5 σ from the region occupied by late-type stars. The average colors of the sample are quite similar to those of either a main-sequence M3 V, or of M4 Ia supergiants, but do not resemble any single-type class III photosphere. The early spiral types are slightly redder in $J-H$ than the late ones but virtually undistinguishable in $H-K$.

The global NIR colors do not show any clear correlation with the presence of AGNs and bars (see Sect. 3.4), or with the position within the cluster. Nevertheless, the $H-K$ colors of two of the three Seyferts are among the reddest in the sample. Red $H-K$ colors coupled with normal $J-H$ are indeed typical for Seyfert galaxies (Spinoglio et al. 1995), but the excess in $H-K$ depends on the AGN luminosity and dilution by the host galaxy. Hence, the lack of a definitive NIR global color signature for AGNs is not surprising.

[6] We report on the plot only the errors estimated by us on $(J-K)_{21.5}$; the average uncertainty on $B_{\rm T}-J_{21.5}$ is expected to be of the same magnitude or slightly (0.1 mag) worse.

[7] The Galactic reddening has been computed from the $A_{\rm B}$ values listed in NED and the Cardelli et al. (1989) reddening curve.

Table 2. NIR global and disk colors

Name (1)	$H_{21.5}$ (2)	$D_{21.5}$ (3)	$2 \cdot r_{BD}$ (4)	$(J-H)_{21.5}$ (5)	$(H-K)_{21.5}$ (6)	σ_{JK} (7)	$(J-H)_D$ (8)	$(H-K)_D$ (9)	$\delta(J-K)$ (10)
UGC 12914	9.52	2.40	0.33		0.55 ± 0.18			0.47	
UGC 12915	10.48	1.71	0.15		0.65 0.18			0.55	
UGC 00365	9.58	1.84	0.29		0.34 0.14			0.27	
UGC 00646	10.73	1.42	0.22	0.76 ± 0.22	0.23 0.20	± 0.21	0.72	0.22	
UGC 00673	12.73	0.55	0.00	0.71 0.05	0.26 0.08	0.07	0.71	0.26	0.18 ± 0.06
CGCG 501-091	13.15	0.49	0.16	0.56 0.09	0.21 0.05	0.09	0.48	0.19	
UGC 00697	11.04	1.26	0.17	0.63 0.09	0.22 0.05	0.09	0.59	0.26	0.03 0.03
UGC 00710	11.71	1.41	0.12	0.78 0.09	0.32 0.05	0.09	0.75	0.33	−0.22 0.07
UGC 00714	11.30	1.08	0.08	0.62 0.05	0.33 0.07	0.08	0.60	0.29	−0.06 0.02
UGC 00732	11.29	1.27	0.14	0.70 0.06	0.27 0.05	0.06	0.69	0.27	0.06 0.02
UGC 00738	12.16	0.96	0.22	0.76 0.08	0.24 0.05	0.08	0.70	0.20	
UGC 00745	14.28	0.32	0.00	0.64 0.06	0.37 0.08	0.08	0.64	0.37	
UGC 00776	10.28	1.12	0.31	0.72 0.04	0.22 0.04	0.05	0.74	0.21	0.15 0.04
UGC 00798	11.30	1.05	0.18	0.68 0.09	0.32 0.14	0.15	0.70	0.25	−0.18 0.06
UGC 00800	12.67	0.65	0.00	0.60 0.04	0.22 0.03	0.04	0.60	0.22	−0.04 0.05
UGC 00820	9.54	2.75	0.32	1.04 0.22	0.18 0.20	0.21	0.99	0.11	−0.16 0.03
CGCG 502-021	13.02	0.57	0.12	0.60 0.08	0.22 0.05	0.08	0.57	0.20	
UGC 00831	12.58	0.58	0.13	0.61 0.04	0.29 0.03	0.04	0.56	0.22	−0.11 0.03
UGC 00835	12.04	0.73	0.06	0.70 0.06	0.26 0.05	0.06	0.70	0.25	
CGCG 502-032	12.33	0.77	0.09	0.80 0.07	0.19 0.07	0.07	0.74	0.20	0.03 0.09
UGC 00909	11.95	0.94	0.20	0.62 0.06	0.31 0.06	0.06	0.58	0.34	0.12 0.04
UGC 00911	11.76	0.75	0.06	0.71 0.09	0.40 0.14	0.15	0.67	0.32	−0.01 0.05
UGC 00919	9.60	2.33	0.21	0.75 0.05	0.30 0.08	0.07	0.70	0.27	0.10 0.05
UGC 00927	11.14	1.41	0.14	0.37 0.21	0.52 0.17	0.21	0.30	0.50	−0.17 0.02
UGC 00937	12.01	0.75	0.00	0.72 0.09	0.26 0.14	0.15	0.72	0.26	−0.18 0.06
UGC 00940	12.33	0.86	0.14	0.49 0.10	0.40 0.11	0.13	0.45	0.35	−0.06 0.05
UGC 00975	12.21	0.88	0.22	0.68 0.06	0.26 0.06	0.06	0.61	0.24	−0.20 0.05
UGC 01013	9.52	2.43	0.61	0.46 0.21	0.41 0.17	0.21	0.43	0.36	−0.03 0.05
CGCG 502-085	11.73	0.72	0.08	0.62 0.09	0.45 0.05	0.09	0.57	0.48	0.20 0.06
UGC 01034	10.33	1.71	0.12	0.75 0.10	0.22 0.08	0.12	0.65	0.30	−0.07 0.02
CGCG 521-038	13.74	0.42	0.00	0.54 0.09	0.30 0.05	0.09	0.54	0.30	−0.65 0.08
CGCG 502-097	12.88	0.70	0.00	0.60 0.09	0.32 0.05	0.09	0.60	0.32	
UGC 01100	10.14	2.21	0.29	0.71 0.08	0.23 0.13	0.15	0.70	0.14	−0.47 0.11
UGC 01111	10.20	1.26	0.21	0.66 0.04	0.33 0.05	0.05	0.62	0.32	−0.09 0.03
UGC 01131	12.23	0.81	0.15	0.71 0.09	0.17 0.10	0.08	0.74	0.15	0.03 0.05
CGCG 521-068	11.87	0.62	0.13	0.72 0.06	0.16 0.05	0.07	0.68	0.06	−0.46 0.08
CGCG 503-007	12.89	0.54	0.00	0.61 0.04	0.38 0.05	0.05	0.61	0.38	0.24 0.08
UGC 01437	9.76	1.48	0.25		0.27 0.11			0.30	
UGC 01633	9.50	2.37	0.24		0.24 0.10			0.28	
UGC 01935	9.22	4.10	0.32		0.44 0.20			0.28	
UGC 02548	9.85	1.62	0.38		0.51 0.15			0.53	

3.2. Bulge and disk colors

For each galaxy we define a radius, $r_{\rm BD}$ in arcmin (Col. 4 in Table 2), where the disk contribution becomes dominant. This is a visual estimate from the H-band profiles (Paper I) of the point were the radial surface-brightness profile, averaged over elliptical isophotes, becomes disk-like (straight on a log-linear plot). From simulations performed on a variety of synthetic bulge+disk systems, $r_{\rm BD}$ is on average equivalent to the point were the the bulge surface magnitude fades to about 3 mag below the disk one. Some of the galaxies do not show any central bump in surface brightness, that is no evident bulge; these are the systems labeled as "pure disk" in Table 1 and with $r_{\rm BD} = 0$ in Table 2. These objects are either spirals of the latest types or lacking a precise Hubble type. Their global NIR colors are statistically undistinguishable from the rest of the set.

We have recomputed the NIR colors for the regions comprised between $r_{\rm BD}$ and the $21.5\,H$-mag arcsec^{-2} isophote. These "disk" colors are reported in *Columns* 8 and 9 of Table 2 as $(J-H)_{\rm D}$ and $(H-K)_{\rm D}$; their uncertainties are basically the same reported for the global colors. The right panel of Fig. 5 shows the color-magnitude relation when using the disk color $(J-K)_{\rm D}$ and the isophotal (global) luminosity. The correlation, if any, is substantially worse than for the global color and it degrades further if we use linear sizes (either optical or NIR) as "luminosity" indicators. This probably reflects the fact that most of the correlation observed between $(J-K)_{21.5}$ and absolute magnitude is due to the correlation present in the sample between luminosity and morphology (cf. Fig. 2). These issues will be addressed in a forthcoming paper of the series in the context of decomposition into bulge and disk components.

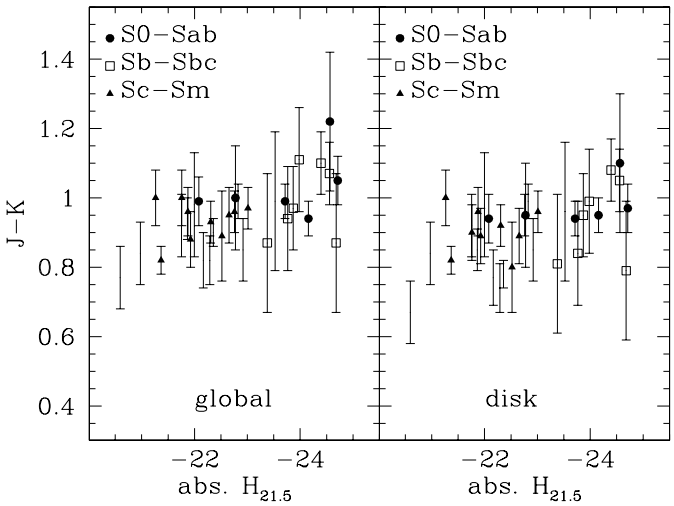

Fig. 5. NIR color-magnitude relation. The global isophotal color $(J-K)_{21.5}$ (right panel) and the disk color $(J-K)_{\rm D}$ (left panel) vs. the absolute $H_{21.5}$ (global) magnitude. Absolute magnitudes are computed assuming simple redshift distances, with $H_0 = 75$ km s^{-1}Mpc^{-1}. The figure format is the same of Fig. 4

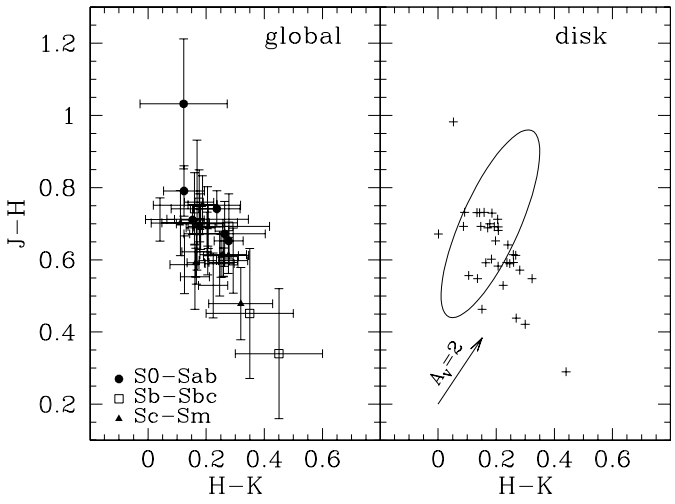

Fig. 6. NIR color-color diagram. In the left panel the global isophotal color $(J-H)_{21.5}$ is plotted vs. $(H-K)_{21.5}$; for each point we report also the 1σ errors and the different types are coded as in Fig. 4. In the right panel we plot the disk colors $(J-H)_{\rm D}$ vs. $(H-K)_{\rm D}$ with the same symbol for all types; the reddening line is shown in the lower left corner and the ellipse encompasses the region occupied by stars from K0 to M5 of all luminosities from I to V. The colors shown here have been corrected for K-dimming and Galactic extinction

The NIR color-color diagram of disks is shown in the right panel of Fig. 6. The points lie in the same region of the global colors with only a slight average shift to the blue of about 0.03 mag in both colors. The left panel of Fig. 7 shows the difference between the global $(J-K)_{21.5}$ and disk $(J-K)_{\rm D}$ colors as a function of the morphological index T. While the value of this difference depends both on the difference in color between bulge and disk and on the bulge-to-disk luminosity ratio B/D, its sign will be positive if the bulge is redder than the disk, and negative otherwise. Clearly, the NIR color of bulges is redder than in disks, as evidenced also by the radial color profiles in Fig. 3; no bulges bluer than their disk are observed within the photometric uncertainty. That $J-K$ is redder in the central regions of high surface brightness recalls earlier results for early-type spirals which tend to have bulges roughly 0.1 redder in $J-K$ than their disks (Moriondo et al. 1998a); see Peletier et al. (1999) for recent Hubble Space Telescope NICMOS observations. In the right panel of Fig. 7, the same color difference is plotted vs. the light concentration index C_{31} from Paper I (H band)[8]. C_{31} depends on the galaxy absolute luminosity and, to a lesser degree, on morphology (Gavazzi et al. 1996). We find no trend of $(J-K)_{21.5}-(J-K)_{\rm D}$ with the NIR concentration index. Given the size of the errorbars in Fig. 7, we find no definite trend with morphology. We note, however, that the smallest differences are attained by the earliest and latest spiral types. In late types this is due to the low B/D ratio, in early types to the redness of their disks (cf. Fig. 5).

[8] C_{31} is the ratio of the major axes of the elliptical isophotes enclosing 75% and 25% of the flux corresponding to $H_{21.5}$ (Gavazzi et al. 1990).

The few objects hosting active nuclei do not show an extreme $J-K$ color difference; the largest, although with a rather large error, is attained by UGC 831 and 911 at $(J-K)_{21.5}-(J-K)_{\rm D} = 0.12$. Upon inspection of the radial color profiles, unresolved blue nuclei (not bulges) are found only in the members of the interacting pair VV254, UGC 12914 and 12915, which have for the rest a quite red $H-K$ color. A very red nucleus shows up in the $H-K$ color image and profile of the Sy 1.5 UGC 1935; notably also the color difference $(H-K)_{21.5}-(H-K)_{\rm D} = 0.16$ of this galaxy is the largest of the sample.

The radial color profiles of some objects with a well defined bulge (UGC 646, 776, 919, 927, 1013, 1633, and 2548) are characterized by a blue dip at the "transition" between bulge and disk. We find few elements in common among these objects: some are early spirals and others late, some have bars and some have none. Apart from this feature, their colors are quite normal and span through the whole range observed. The dip, which is best evident in the $J-H$ profiles, is usually observed in large galaxies, both in angular and linear size. It is not clear, from our data, whether this is due to the better spatial resolution or is rather a characteristic of giant spirals. The only common element which we find among these blue-dip galaxies is that they are all endowed with a conspicuous lens component (Sandage 1961) as noticeable in their H-band images and also from the plateau in their brightness radial profile in Paper I. The location of the blue minimum coincides with the transition between bulge and lens and is much more internal than the onset of well-defined spiral arms. It is not clear from our data whether

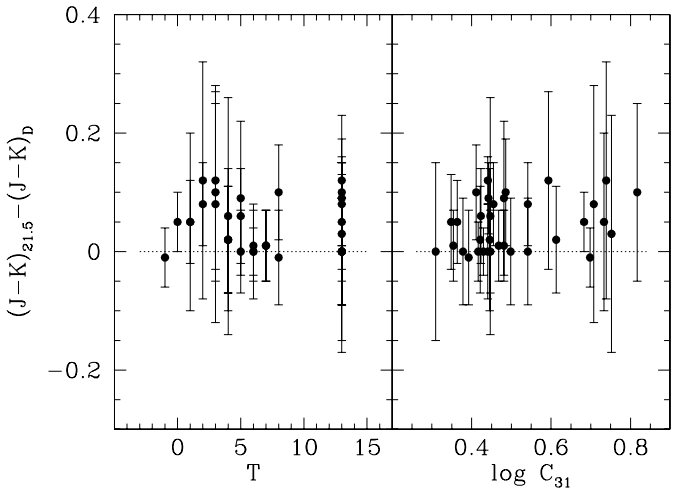

Fig. 7. The difference between the global color $(J-K)_{21.5}$ and the disk one $(J-K)_{\rm D}$ as a function of morphological index T (left panel), and of the concentration index C_{31} (right panel). In the left panel, the points at $T = 13$ refer to objects classified S or SB without further specification

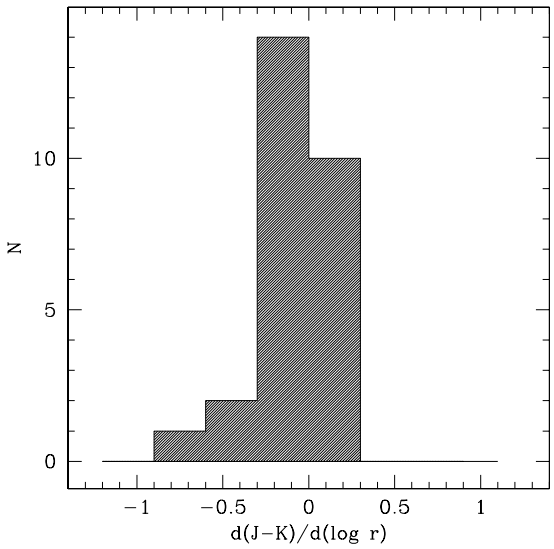

Fig. 8. Distribution of the $J-K$ radial color gradient in the disk dominated region of the galaxies. Only gradients determined with confidence are reported. Gradients are defined as $d(J-K)/d(\log_{10} r)$, where r is the major semiaxis of the elliptical isophote

the effect is due to an excess of blue emission or to a lack of red one.

3.3. Disk color gradients

We only examine $J-K$ color gradients in the disk region. As customary (e.g. Terndrup et al. 1994), the color gradient is defined as $\delta(J-K) = d(J-K)/d\,\log_{10} a$, where a is the semimajor axis of the elliptical isophote. We have computed them with a weighted regression in the range $r_{\rm BD} \le a \le r_{21.5}$[9], with weights $1/\sigma^2$, where σ is the uncertainty on the local, elliptically averaged, color. We only consider gradients determined either with confidence better than 3σ or, for values near zero, with $\sigma \le 0.05$; their values are reported in Col. 10 of Table 2.

The distribution of the disk gradients is shown as a histogram in Fig. 8. Within our precision, most of values cluster around zero, with only a slight tendency toward negative values. We find no clear dependence of the NIR radial color gradient of the disk on any galaxy attribute. As shown in Fig. 9, the value of $\delta(J-K)$, or even its sign, does not depend on the galaxy morphological type, nor on the galaxy luminosity (left panel); if anything, we may note (right panel) a slight tendency for the most positive $\delta(J-K)$ values to be found in red disks.

The variation of the NIR color with location within the galaxy is further illustrated by Fig. 10. Here we report, for all the sample galaxies together, the $J-K$ color at each isophotal level (from elliptical fitting) vs. the H surface magnitude in the left panel, and vs. the corresponding distance from center, normalized to $r_{21.5}$ in the right panel; only points with error on $J-K$ better than 0.2 are shown. Although with some scatter, the reddest colors are observed at small galactocentric distance and bright surface brightness in regions still dominated by bulge emission. Most of the points are clustered in an intermediate range ($17 < \mu_{\rm H} < 20$) with a very tight color distribution around $J-K \simeq 0.95$. The outer, and fainter, regions have a looser distribution, also due to the larger photometric errors, with a definite shift to bluer colors only in some of the sample objects.

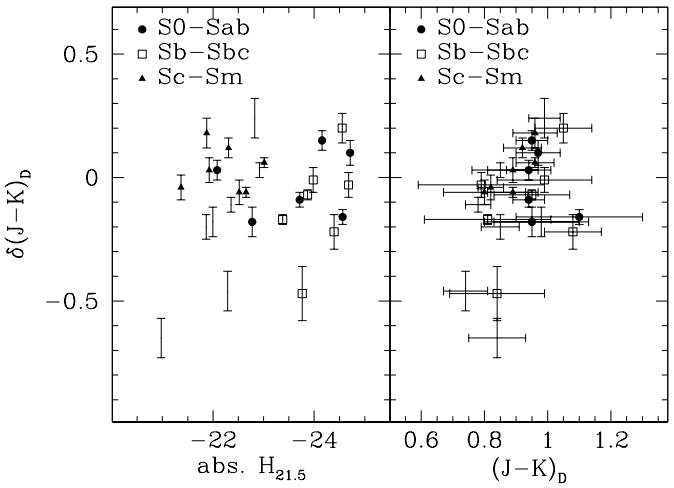

Fig. 9. Left panel: the $J-K$ radial color gradient in the disk $\delta(J-K)_{\rm D}$ vs. the absolute $H_{21.5}$ magnitude of the galaxy. Right panel: $\delta(J-K)_{\rm D}$ vs. the disk $J-K$ color. The points are coded as in Fig. 4. As in Fig. 8, only reliable gradient measurements are reported

3.4. Structure in the color images

The $J-H$ and $J-K$ images shown in Fig. 3 are remarkable for their lack of large scale structure. In particular, bars, which are evident in the surface brightness image and

[9] $r_{21.5} = D_{21.5}/2$.

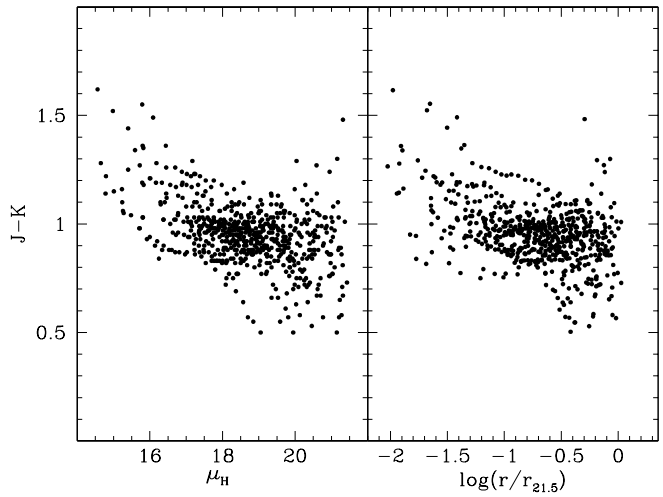

Fig. 10. Left panel: local $J-K$ color vs. local H-band surface brightness in mag arcsec^{-2}. Right panel: local $J-K$ color vs. radius normalized to the H-band isophotal size. Local quantities are defined by elliptically averaging the brightness distributions as explained in Sect. 3. All the available points, with a $J-K$ error below 0.2 mag, for all the sample galaxies are reported in these graphs

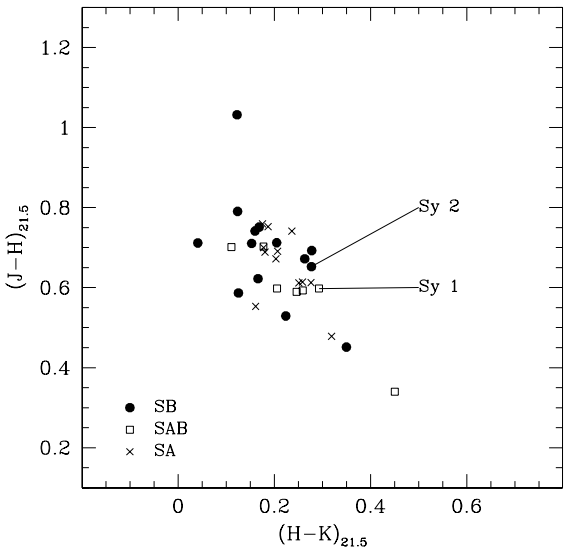

Fig. 11. NIR color-color plot. As in Fig. 6 but with different symbols for different bar types; also evidenced are the two AGN hosts for which the colors are available

in the radial ellipticity profiles (Paper I), have no signature in the NIR colors. As noted previously, the presence of bars is also of scarce relevance for the global NIR colors of a galaxy, as is the presence of an active nucleus; both facts are clearly illustrated by Fig. 11. This is a somewhat different situation than in the optical waveband where strong bars are frequently delineated by sharp parallel dust lanes (e.g. Binney & Tremaine 1987). In general, anyway, the bar stellar content itself in not evident either in the optical (Wozniak et al. 1995) or in the NIR (Shaw et al. 1995; Friedli et al. 1996). Stellar bars appear therefore to be relatively evolved features. On the other hand, spiral structure (e.g. UGC 831), bulge-lens transitions (e.g. UGC 927), and twisted isophotes (e.g. UGC 12914) present some structure in the NIR color images. Spiral structure in M51 has been found to have an arm-interarm contrast $\Delta(J-K) \simeq 0.15$ (Rix & Rieke 1993) which is consistent with the values we measure in UGC 831. Lenses and twisted isophotes tend to be found in early-type spirals, so the paucity of these in our sample precludes definitive statements, except for the blue dips noted in Sect. 3.2. The color variations $\Delta(H-K)$ and $\Delta(J-K) \sim 0.15$, seen in some of our color images, may also be characteristic of these structures.

4. Summary

1. We present NIR color images for a sample of 41 disk galaxies in the Pisces-Perseus supercluster area: $J-H$ and $J-K$ images for 34 of them and $H-K$ for the remaining 7. The sample objects were drawn from a larger set of 174 galaxies in the area whose H-band imaging has been reported and used in previous papers of this series. The sample objects are mostly members of the Pisces cluster;
2. The $J-K$ (global) color correlates weakly with absolute luminosity and morphological type. We observe no trend with the presence of bars and AGNs, nor with position within the cluster;
3. The NIR disk colors are slightly bluer than the global ones, with the possible exception of those in the earliest spiral types. Hence, in the NIR, bulges are slightly redder than disks, confirming earlier work (Moriondo et al. 1998a). Redder $J-K$ is observed at the small galactocentric distances and bright surface brightness regions dominated by the bulge;
4. NIR disk color gradients are small and prevalently negative. We find no trend between these gradients and other galaxy attributes; possibly, the few positive values are associated with the reddest disks. A blue dip is often observed at the transition between bulge and disk in the luminous members of the sample;
5. Unlike bars, spiral structure and other non-axisymmetric features have a signature in the NIR color images. Blue nuclei are detected in the members of the interacting pair VV 254, and a very red and luminous one in the Sy 1.5 UGC 1935.

Acknowledgements. G. M. warmly acknowledges the hospitality of the Astronomy Dept. of Cornell University, where part of the data reduction was done. We acknowledge the partial support of the Italian Space Agency (ASI) through the grant ARS–98–116/22.

References

Binney, J., & Tremaine, S. 1987, Galactic Dynamics (Princeton Univ. Press, Princeton)
Cardelli, A. J., Clayton, G. C., & Mathis, J. S. 1989, ApJ, 345, 245
Friedli, D., Wozniak, H., Rieke, M., Martinet, L., & Bratschi, P. 1996, A&AS, 118, 461

Frogel, J. A. 1985, ApJ, 298, 528
Frogel, J. A., Persson, S. E., Matthews, K., & Aaronson, M. 1978, ApJ, 220, 75
Gavazzi, G., Garilli, B., & Boselli, A. 1990, A&AS, 83, 399
Gavazzi, G., Pierini, D., Baffa, C., et al. 1996, A&AS, 120, 521
Griersmith, D., Hyland, A., & Jones, T. 1982, AJ, 87, 1106
Moriondo, G., Baffa, C., Casertano, S., et al. 1999a, A&AS, 137, 101 (Paper I)
Moriondo, G., Giovanardi, C., & Hunt, L. K. 1998a, A&AS, 130, 81
Moriondo, G., Giovanelli, R., & Haynes, M. P. 1998b, A&A, 338, 795 (Paper II)
Moriondo, G., Giovanelli, R., & Haynes, M. P. 1999b, A&A, 346, 415 (Paper III)
Nilson, P. 1973, Uppsala General Catalogue of Galaxies, Roy. Soc. Sci. Uppsala, Uppsala (UGC)
Peletier, R. F., Balcells, M., Davies, R. L., et al. 1999, MNRAS, 310, 703
Rix, H.-W., & Rieke, M. J. 1993, ApJ, 418, 123
Sandage, A. 1961, The Hubble Atlas of Galaxies, Carnegie Institution of Washington, Washington
Shaw, M., Axon, D., Probst, R., & Gatley, I. 1995, MNRAS, 274, 369
Spinoglio, L., Malkan, M. A., Rush, B., Carrasco, L., & Recillas-Cruz, E. 1994, ApJ, 453, 616
Terndrup, D. M., Davies, R. L., Frogel, J. A., DePoy, D. L., & Wells, L. A. 1994, ApJ, 432, 518
de Vaucouleurs, G., de Vaucouleurs, A., Corwin, H. G., et al. 1991, Third Reference Catalogue of Bright Galaxies, 3 volumes (Springer-Verlag, New York) (RC3)
Willner, S. P., Ward, M., Longmore, A., et al. 1984, PASP, 96, 143
Wozniak, H., Friedli, D., Martinet, L., Martin, P., & Bratschi, P. 1995, A&AS, 111, 115
Zwicky, F., Herzog, E., Kowal, C. T., Wild, P., & Karpowicz, M. 1961, 1963, 1965, 1966, 1968a,b, Catalogue of Galaxies and of Clusters of Galaxies (6 volumes), Calif. Inst. Techn., Pasadena (CGCG)